POLITECNICO
MILANO 1863

SCUOLA DI INGEGNERIA INDUSTRIALE
E DELL'INFORMAZIONE

Odd - Group 5 Homework Report: 'Preliminary desing and verification of a Fuel Pin'

Course of 'Nuclear Design and Technologies' - MSc. of Nuclear Engineering

Buzzoni Alice, Corbetta Yari, Iaccarino Matteo, Marchesi Davide, Musile Tanzi Marco.

Professors:
Luzzi Lelio,
Pizzocri Davide,
Alessio Magni.

Academic year:
2023-2024

Abstract: This is the final report of the **Group 5** of the **Odd** section for the 2023-2024 Homework project for the course of '*Nuclear Design and Technologies*'. The goal was to perform the preliminary design of a **Sodium-Cooled Fast Reactor's Fuel Pin**, in particular determining the thickness of the cladding, the size of the fuel-cladding gap and the height of the plenum. At the same time should be verified some important constraints dealing both with the thermal and mechanical analysis results (like the yielding, the creep, the margin to melting, and so on...). Our group approached numerically the problem using **Python** language and packages. The script used for the analysis can be found in form of Python notebook (`.ipynb`) at the following link: python notebook. The aim of this report is mainly to critically discuss the results obtained, the assumptions and the process made to have them, and their validity. Some physical/mathematical formulations are given only at the end of the report, in a separated appendix, in order not to make too cumbersome the whole analysis.

Key-words: SFR, Fuel Pin, MOX, Sizing, Plenum, Gap, Thermal Analysis, Mechanical Analysis.

Contents

1. Modeling

In this section we want to illustrate the main models and assumptions made for our '**1.5-D Fuel Pin analysis**', dividing them by topics. The majority of the mathematical passages won't be illustrated, some useful hints are given at the end in A.

1.1. Neutronics

To obtain the best estimates regarding the neutron-nuclei reaction rates a neutron flux energy spectrum was taken from online literature about SFR. The neutrons fraction was significantly greater than zero only within **1keV - 10 MeV**, furthermore above an energy of **100 keV** it was exactly **70%**, as indicated in the data, justifying our choice. To achieve a 1-group cross-section was adopted a group-collapsing approach (as made in ref.[1]) in the above-mentioned energy range, integrating the microscopic cross-section of the isotopes of interest (taken from **JANIS ENDF.B-VII/0** database). Subsequently, the axial neutron flux was computed from both the linear power of the fuel pin and the local isotopic composition of the fuel, finding its intensity in each node along the height of the pin. The product between the neutron flux and the macroscopic cross section would have now led to the reaction rate density, useful to evaluate the production of alpha particles, Xenon and Krypton. The neutronics plots are visible in fig.9,8.

1.2. Power and Coolant

The axial linear power profile of the fuel pin was found by linear interpolation of the data. All along the analysis the power imposed is taken with a step discretization of **1cm**. Using a coolant centered approach and assuming each channel as independent, the coolant axial thermal profile was calculated by solving the energy balance with the power profile of the fuel pin. Null pressure drops were assumed.

1.3. Thermal Analysis

The thermal analysis was performed by considering only radial heat transfer (power imposed) and uniform heat generation in the fuel. The iterative processes involving the temperature profile, the thermal expansion and the fuel restructuring are later described in sec.2.

1.3.1 Cladding and Gap

The outer cladding temperature at each axial point was evaluated using a thermal resistance calculated using average coolant temperature properties. Then by solving heat conduction equation both for cladding and gap, the inner cladding temperature and outer fuel temperature were found (ref.[4]). In addition to this, to calculate a more precise fuel outer temperature also an irradiation model was implemented, considering an **emissivity** of

0.8 for the steel and 0.4 for the fuel. Being already the cladding outer diameter temperature above the design limit, was implemented a **throttling** countermeasure, increasing in this way the flow rate and decreasing the temperature. Thermal expansion of the cladding was then implemented using the tabulated coefficient. In this context, the expanded inner and outer diameter were calculated using the average radial temperature for each axial point, evaluated with an integral average using Simpson's method.

1.3.2 Fuel

The fuel radial temperature profile was found by solving the conduction equation for both fissile and fertile pellets. Then expanded geometry was calculated as described above for the cladding, considering an average integral radial temperature. For what concern the restructuring, the lower limit for the **equiaxed region** is set at **1600°C**, while for temperatures between **1600°C and 1800°C** was considered a **columnar conformation** with a consequent different internal void radius given by the mass balance. The procedure followed is the one depicted in ref.[5]. In the end three different conformations are individuated: zones where the fuel remains as fabricated, zones where the fuel has the creation of only equiaxed grains, and those where an internal void and a columnar region is also created in addition to the equiaxed one.

1.4. Embrittlement

Following the path illustrated by ref.[5] the cladding embrittlement analysis was performed using a set of Bateman equations. As made for the neutrons flux also here was used **JANIS ENDF.B-VII/0** (ref.[3]) database for the elements cross sections estimation. Before proceeding with the calculations, were selected only those isotopes that satisfy both the following criteria: not negligible atomic concentration and not too small nuclear reaction cross section (only ($\boldsymbol{n \rightarrow \alpha}$), or radiative capture ($\boldsymbol{\gamma}$) were accounted). In the end were considered: $\boldsymbol{Ni_{58/59/60}}$, $\boldsymbol{Fe_{54/56}}$, $\boldsymbol{B_{10}}$, $\boldsymbol{Cr_{52}}$. The set of differential equations was solved obtaining both the average and the local (axial) **Helium** buildup in the cladding.

1.5. Burnup - Fission Gas Production

Using the time evolution of the power from the tabulated data (**-10%** every **360EFPD**) the Burnup of the fuel is calculated starting from the above described neutronic approach (1.1). The strong assumption made is that the isotopic composition of the fuel, for both **'Pu'** and **'U'**, do not change in time. A more accurate treatment would need a more sofisticated model accounting also for neutronic feedbacks. Though, this first approximation for the purposes of the pin design is not very gross: the lack of the description of the produced Plutonium in the fertile elements is compensated by the absence of the Plutonium depletion in the fissile elements. The Burnup calculation is then used to estimate the fission gas release. We assumed a contribute as fission gas release of only **Xenon** and **Krypton**, assumed to have respectively a yielding of: $\gamma_{Xe} = 27\%$, $\gamma_{Kr} = 3\%$ (accounting for a cumulative value of all the possible isotopes).

1.6. Plenum Sizing

In order to safely dimensioning the plenum a **100% release** of fission gases from the fuel to the gap is assumed (no retention). This, together with the model adopted for the burnup (no 'Pu' and 'U' consumption), leads to a simplified but conservative model. The more reasonable choice to design the plenum is to use a lower unique one, in such a way that the equilibrium temperature of the gas corresponds with the one of the coolant at the inlet, limiting in this way the effect of pressurization (this can be made simply by using an upper isolating plate). Furthermore is assumed that the gas mix will be in thermodynamic equilibrium in this lower part, responding to the **classical ideal gases equations**. Once that the initial filling conditions are known, are analyzed different possible sizes of the plenum such that the safety limit of **5MPa** at the end of life is respected.

1.7. Stress-Strain Analysis

The stress-strain analysis was conducted using the **Lamé** approach to evaluate the thermo-mechanical state of the cladding. The investigation was performed using the hypothesis of **orthocylindricity** and **axial symmetry**, exploiting the principle of superposition between the two effects (thermal and mechanical) to compute the final stress state condition. In order to develop the calculations, the boundary conditions were known a priori thanks to the other simulations made (i.e. the pressure acting on the pin). The axial mechanical stress, in particular, was calculated using a force balance on the z-axis, assuming realistic additional external forces

acting on the cladding: the elastic force of the spring and the weight of the cladding itself. The contact pressure was evaluated by means of the interference between the outer fuel and cladding inner radii (ref.[2]). In the end the final verification with respect to the **yielding stress** was made using the **Tresca criterion**.

1.8. Creep-Swelling

For both the **thermal** and **irradiation creep** effects were used the tabulated correlations, computing its rate, in order to verify in the end the given constraints. The **void swelling**, for both the fuel and the cladding, was evaluated directly using the given correlations, and then superposed to the thermo-mechanical strains.

2. Code Structure

Axial nodes	Radial nodes	Time step	Tolerance
110	200	1 day	1e-7 (m)

Table 1: Simulation parameters

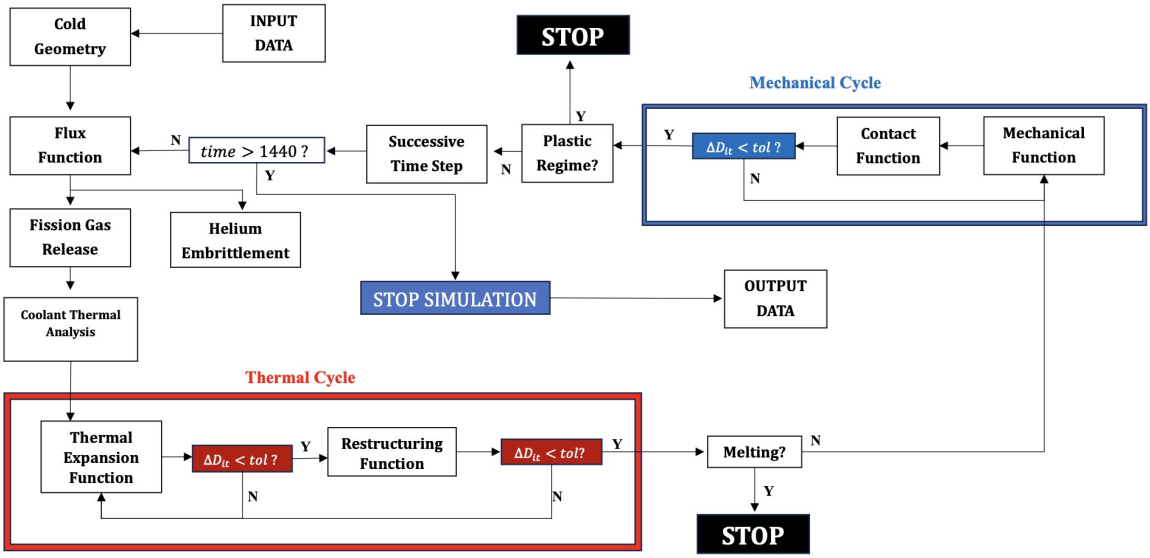

Figure 1: Code's block diagram

The whole code was implemented in the **COLAB IDLE**, using **Python** language and online packages. The structure is the one illustrated in fig.1. The code starts having as input the **cold geometry analysis**. Then the temporal cycle starts. First of all at each temporal step is calculated the flux, which takes as input the information about the power and the cross sections (as explained in (1.1)). From this, are extrapolated the data about the fission gas release (**Xe-Kr** concentration, gap conductivity, and internal pressure) and the embrittlement (isotopic conformation of the cladding).
Then the thermal analysis is performed: after the coolant and of the cladding outer diameter temperature calculation, the temperature profile at each axial and radial point is performed. The **thermal expansion function** takes as an input the outer temperature of the cladding, extrapolating the new hot geometry profile accounting for both the thermal expansion and the swelling effects. An iterative cycle to reach convergence is made, and then the output is used subsequently to make the restructuring calculation with the **restructuring function**. Another iterative cycle is performed, in order to reach convergence, on the whole thermal analysis. The output is compared to the upper fuel temperature limit admitted, in case this threshold is exceeded the code is interrupted, otherwise the calculation proceeds.
The last step involves the **mechanical analysis**. Using the thermal output in the **mechanical function** a stress-strain evaluation is made. The output is used to verify the contact, and eventually compute the new pressure, between the fuel and the diameter with the **contact function**. Also here an iteration to reach a numerically stable and physically reasonable result is made. In the end a check on the yielding stress is done.

In case of positive response the time iteration proceeds to the successive temporal step. The simulation ends at the end of the 1440th EFPD of operation of the fuel pin.

3. Results

The following plots and data are the results of the following design parameters:

Cladding Thickness	Gap Thickness	Plenum Height	Mean Mass Flow Rate
420 μm	200 μm	1 m	0.0925 kg/s

Table 2: Design parameters

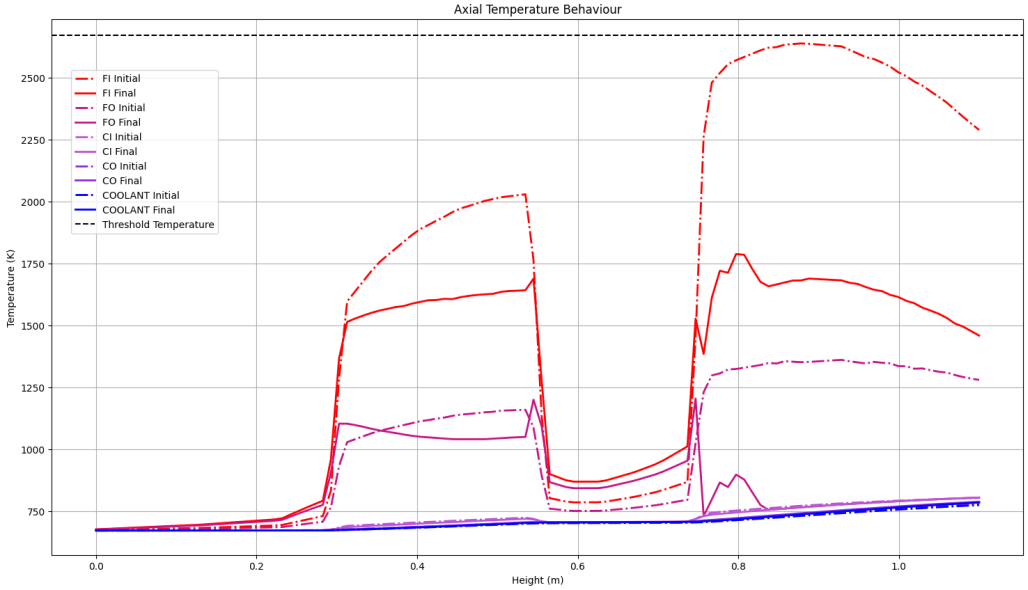

Figure 2: Axial Temperature plot

As can be seen in fig.2 the temperature profile follows the linear power one. While the cladding profile changes only slightly from the initial condition only due to the power changes in time, the initial and final profiles of the fuel differ a lot. The variation occurs due to the gap thickness change in time as visible in fig.4. The general flattening trend in the first fissile pellet, axially, is connected to the thermal expansion phenomenon, higher in the upper part, leading to a thinner gap, and thus a lower gap thermal resistance . In the second fissile element persists the typical trend of the power due to the contact with the cladding, resulting in the outer fuel temperature being equal to the inner cladding one. In the final instant the maximum is only given by those points in the upper fissile element not in contact with the external part.

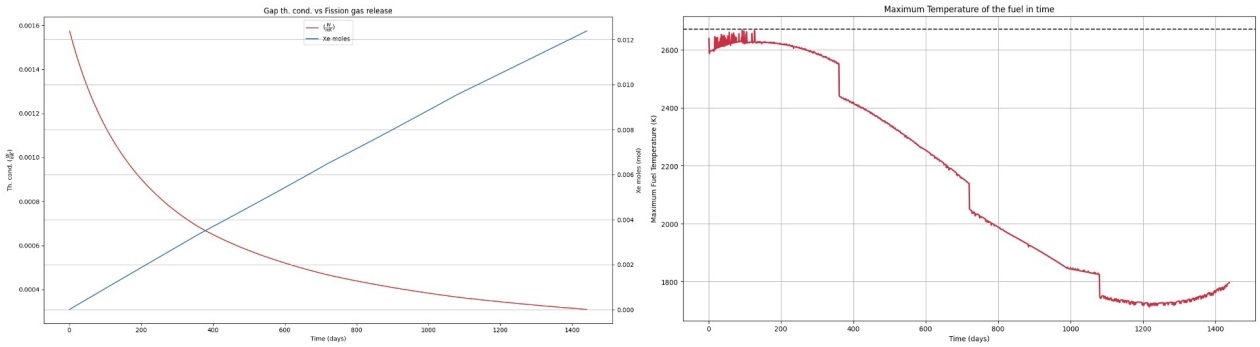

Figure 3: Maximum Fuel Temperature and Gas thermal conductivity in time

The maximum temperature reached, as depicted in fig.3, remains below the design limit (2396.37°C < 2400.00°C). Even if it appears to be pretty near the upper threshold, as visible above this is only due to numerical fluctuations in the first part, and the difference in reality would be higher. In the first part a positive trend occurs due to the high change of thermal conductivity lead by the initial production of Xenon and Krypton (fig.3), which is contrasted in first place by the thermal expansion of the fuel, reducing the gap thickness, and in second place by the restructuring effect, leading to a progressively larger formation of the central void (as visible in fig.6 in the appendix). Once that these effects are stabilized, the continuous approaching of the pellet towards the cladding reduces gradually the temperatures. The steps appearing in the curve are caused by the model adopted for the reduction of power due to the annual refuelling (−10% of power every 360 EFPD).

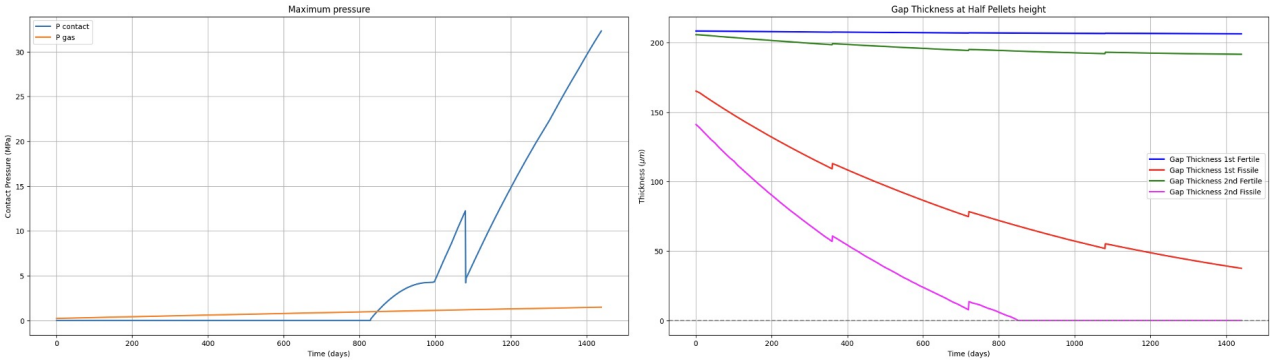

Figure 4: Pressure and Gap Thickness in time

Observing the behaviour of the inner pin pressure in fig.4 is evident the predominant effect of the contact pressure with respect to the fission gas one, becoming the main responsible of the mechanical stresses. The contact appears only at the beginning of the 3^{rd} year, and the behaviour of this one, as predicted, is a ramp, with a step decrease at the 1080^{th} EFPD due to the power change. Looking at the gap thickness in the second image is also possible to observe (as also in 6) that the fuel touches the inner cladding only in the upper fissile pellet. In the lower fissile one on the other hand the contact still not appears, as in the fertile ones, due to the more favorable conditions in terms of neutron flux and temperatures. The worst condition for what concern the stress state is thus obtained in the upper pellet, and is the one represented in fig.5

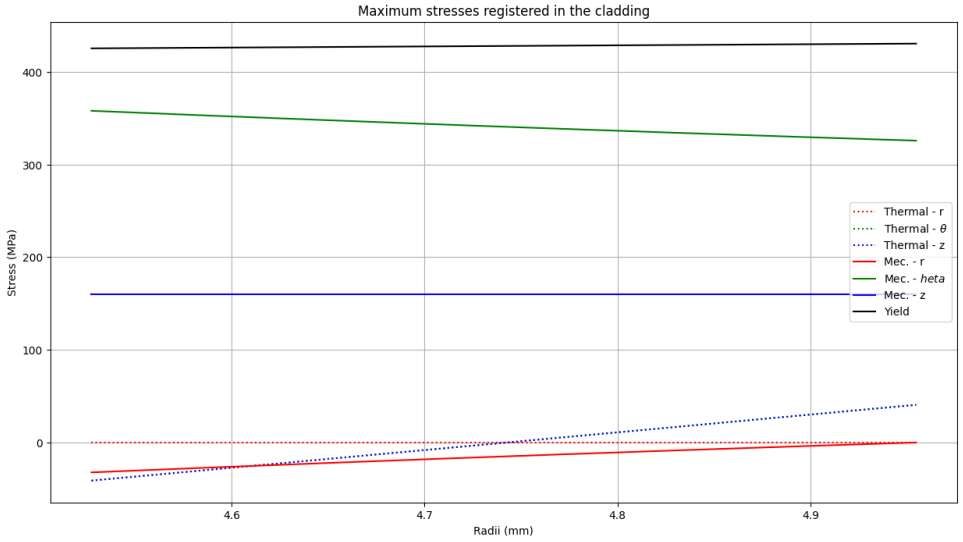

Figure 5: Worst Stress State condition of the cladding (radial plot)

In this case is possible to see how the mechanical stress becomes predominant to the thermal one because of the high pressure of contact achieved, without exceeding the threshold given by the Yielding stress. The stress states are also used to evaluate the thermal and creep irradiation effects, represented in fig.7

4. Final Discussion

The values selected for the pin design are the ones in table 2, with which were obtained the numerical results. All the design limit conditions (as appreciable in table 3) appear to be respected.

Table 3: **Numerical Results vs Design Limits**

Physical Quantity	Code Result	Design Limit
Max. Fuel Temperature	2396.37°C	2400.00°C
Max. Clad Mid Temperature	545.30°C	620.00°C
Max. Plenum Pressure	1.48 MPa	5 MPa
Max. Clad Th. Creep Strain	7.6e-3%	0.2%
Cladding Vol. Swelling	5.68%	6%
Tresca σ_{eq}	393.22 MPa	430.62 MPa
Helium	37.6 ppm	100 ppm

The designing was made executing several simulations, and selecting the best parameters respecting both the thermal and mechanical constraints. The range of the possible gap thicknesses around the value of $200\mu m$ is actually little and constrained in 'both directions' (increasing or decreasing the dimension) because of different effects : a thicker gap would bring the maximum temperature nearer the upper limit, while a thinner one would make overcome the yield stress. This gap size then gives us a little margin from the thermal point of view, accounting also for the numerical fluctuations, and a margin from the mechanical point of view, without entering the plastic regime. In order to have a higher margin from the design constraints also other two hypothesis were made: a upper mass flow rate, from the beginning of life, with respect to the indicated one, and a higher Helium content, leading to a an oversizing of the plenum. The first one is made considering a gradual throttling condition of the hot channel, characterized from the beginning of life by an higher value of sodium flow with respect to the reactor's average one. The second one, about the plenum, was made to guarantee a larger thermal conductivity at the beginning of life, when the most critical thermal condition is reached. This causes an over-design of the plenum height which could be avoided pressurizing the pin at the beginning of life. In fact, under the hypothesis of 2 bar of Helium pressure would be possible to have a plenum of half the height adopted in the simulation, doubling the final pressure obtained. Though was decided to not pressurize remaining in a more conservative condition.

In the end we can consider the results to be pretty satisfying: the design limits were respected using a simulation accounting in contemporary on all the thermo-mechanics effects indicated, with their reciprocal feedbacks, and obtaining realistic parameters for the fuel pin design. Some approximations, physically motivated, were made, which compensate on the other hand for the lack of an accurated neutronics and thermal-hydraulics simulations, together with the propagation of numerical errors.

Thanks for reading.

References

[1] Louis J. Hamilton James J. Duderstadt. *Nuclear Reactor Analysis*. 1976.

[2] Lelio Luzzi. *Nuclear Design and Technologies Miscellaneous material*. 2023-2024.

[3] NEA. Janis, 2020.

[4] Mujid S. Kazimi Neil E. Todreas. *Nuclear Systems - Volume 1: Thermal Hydraulics Fundamentals*. 2021.

[5] Donald R. Olander. *Fundamental Aspects of Nuclear Reactor Fuel Elements*. 1976.

A. Mathematical Appendix

A.1. Neutron Flux Calculations

A.1.1 Group Collapsing Approach

$$\Sigma = \frac{\int_{E_0}^{E_1} \Sigma_1 \Phi(E) dE1 \ + \ \dots \ + \ \int_{E_{n-1}}^{E_n} \Sigma_n \Phi(E) dEn}{\int_{E_0}^{E_1} \Phi(E) dE1 \ + \ \dots \ + \ \int_{E_{n-1}}^{E_n} \Phi(E) dEn} \tag{1}$$

A.1.2 Local Flux Calculation

$$\Phi(z) = \frac{q'(z)}{wA_{sec}\Sigma_f C} \quad \rightarrow \quad \begin{cases} \Sigma_f = \Sigma_f^{U235} + \Sigma_f^{U238} & \text{if : FERTILE;} \\ \Sigma_f = \Sigma_f^{U235} + \Sigma_f^{U238} + \Sigma_f^{Pu} & \text{if : FISSILE.} \end{cases} \tag{2}$$

A.1.3 Xenon and Krypton Calculation

$$\begin{cases} Kr = \gamma_{Kr} V_{fuel} \sum_{Pu_i,U_i} (\Phi \Sigma_{Pu_i,U_i} cf \frac{N_i MM_{Kr}}{N_a v}); \\ Xe = \gamma_{Xe} V_{fuel} \sum_{Pu_i,U_i} (\Phi \Sigma_{Pu_i,U_i} cf \frac{N_i MM_{Xe}}{N_a v}). \end{cases} \tag{3}$$

A.2. Coolant Heat Transfer

$$Nu = 7 + 0.025 Pe^{0.8} \quad \rightarrow \quad R_{cool} = \frac{1}{D_{c,out} \pi HTC} \quad \rightarrow \quad T_{c,out}(z) = T_{cool}(z) + q'(z) R_{cool} \tag{4}$$

A.3. Cladding and Gap Heat Transfer

A.3.1 Cladding Heat Transfer

$$\frac{q'(z)}{2\pi r} = -k_{cl}(T) \frac{dT}{dr} \tag{5}$$

A.3.2 Gap Heat Transfer

$$\begin{cases} \textbf{Conduction:} & \frac{q'(z)}{2\pi r} = -k_{gap}(T) \frac{dT}{dr}; \\ \textbf{Irradiation:} & \frac{q'(z)}{2\pi r} = \frac{A_f \sigma_b (T_f^4 - T_c^4)}{\frac{1-\epsilon_f}{\epsilon_f} + \frac{1}{F_v} + \frac{1-\epsilon_c}{\epsilon_c} \frac{A_f}{A_c}}. \end{cases} \tag{6}$$

A.4. Fuel Restructuring

$$\begin{cases} \frac{1}{r} \frac{d}{dr} \left(r k_{asf} \frac{dT}{dr} \right) = -q'''_{asf} & \text{for: } r \in [R_{eq}, R_{fo}] \\ \frac{1}{r} \frac{d}{dr} \left(r k_{eq} \frac{dT}{dr} \right) = -q'''_{eq} & \text{for: } r \in [R_{col}, R_{eq}] \\ \frac{1}{r} \frac{d}{dr} \left(r k_{col} \frac{dT}{dr} \right) = -q'''_{col} & \text{for: } r \in [R_{void}, R_{col}] \\ \\ (R_{fo}^2 - R_{fi}^2) \rho_{asf} = (R_{col}^2 - R_{void}^2) \rho_{col} + (R_{fo}^2 - R_{col}^2) \rho_{asf} \end{cases} \tag{7}$$

A.5. Embrittlement Bateman Equations

$$\begin{cases} \frac{dNi_{58}}{dt} = -(\sigma_{\gamma}^{Ni_{58}} + \sigma_{\alpha}^{Ni_{58}})\Phi Ni_{58}; \\ \frac{dNi_{59}}{dt} = \sigma_{\gamma}^{Ni_{58}}\Phi Ni_{58} - \sigma_{\alpha}^{Ni_{59}}\Phi Ni_{59}; \\ \frac{dNi_{60}}{dt} = -\sigma_{\alpha}^{Ni_{60}}\Phi Ni_{60}; \\ \frac{dFe_{54}}{dt} = -\sigma_{\alpha}^{Fe_{54}}\Phi Fe_{54}; \\ \frac{dFe_{56}}{dt} = -\sigma_{\alpha}^{Fe_{56}}\Phi Fe_{56}; \\ \frac{dCr_{52}}{dt} = -\sigma_{\alpha}^{Cr_{52}}\Phi Cr_{52}; \\ \frac{dHe}{dt} = \sum_i \left(\sigma_{\alpha}^{X_i} X_i \Phi\right). \end{cases} \tag{8}$$

A.6. Mechanics

A.6.1 Mechanical Stress-Strain

$$\begin{cases} \sigma_{mec-r} = -\frac{1}{r^2}\frac{(P_{in}-P_{out})}{(\frac{1}{R_{c,in}^2}-\frac{1}{R_{c,out}^2})} + \frac{(P_{in}-P_{out})}{(1-\frac{R_{c,in}^2}{R_{c,out}^2})} - P_{in}; \\ \sigma_{mec-\theta} = \frac{1}{r^2}\frac{(P_{in}-P_{out})}{(\frac{1}{R_{c,in}^2}-\frac{1}{R_{c,out}^2})} + \frac{(P_{in}-P_{out})}{(1-\frac{R_{c,in}^2}{R_{c,out}^2})}; \\ \sigma_{mec-z} = \frac{\pi(P_{in}R_{c,in}^2 - P_{out}R_{c,out}^2)}{\pi(R_{c,out}^2 - R_{c,in}^2)}. \end{cases} \rightarrow \begin{cases} \epsilon_{mec-r} = \frac{1}{E}[\sigma_r - \nu(\sigma_\theta + \sigma_z)]; \\ \epsilon_{mec-\theta} = \frac{1}{E}[\sigma_\theta - \nu(\sigma_r + \sigma_z)]; \\ \epsilon_{mec-z} = \frac{1}{E}[\sigma_z - \nu(\sigma_\theta + \sigma_r)]. \end{cases} \tag{9}$$

A.6.2 Thermal Stress-Strain

$$\begin{cases} \sigma_{th-r} = \frac{\alpha E}{1-\upsilon}\frac{1}{r^2}\left[\frac{r^2-R_{c,in}^2}{R_{c,out}^2-R_{c,in}^2}\int_{R_{c,in}}^{R_{c,out}} T(r)rdr - \int_{R_{c,in}}^{R_{c,out}} T(r)rdr\right]; \\ \sigma_{th-\theta} = \frac{\alpha E}{1-\upsilon}(\bar{T} - T(r)); \\ \sigma_{th-z} = \sigma_{th-\theta} + \sigma_{th-r}. \end{cases} \rightarrow \quad \epsilon_{th} = \alpha(T - T_{ref}) \tag{10}$$

A.6.3 Contact Pressure

$$i = \Delta R_{f,out} - \Delta R_{c,in} - t_{gap} \rightarrow P_{contact} = \frac{i}{R_{c,in}} \frac{1}{\frac{1}{E_{cl}}(\frac{R_{c,in}^2+R_{c,out}^2}{R_{c,out}^2-R_{c,in}^2} + \frac{1}{\nu_{cl}}) + \frac{1}{E_f}(\frac{R_{f,in}^2+R_{c,in}^2}{R_{c,in}^2-R_{f,in}^2} - \frac{1}{\nu_f})} \tag{11}$$

B. Additional Useful Plots

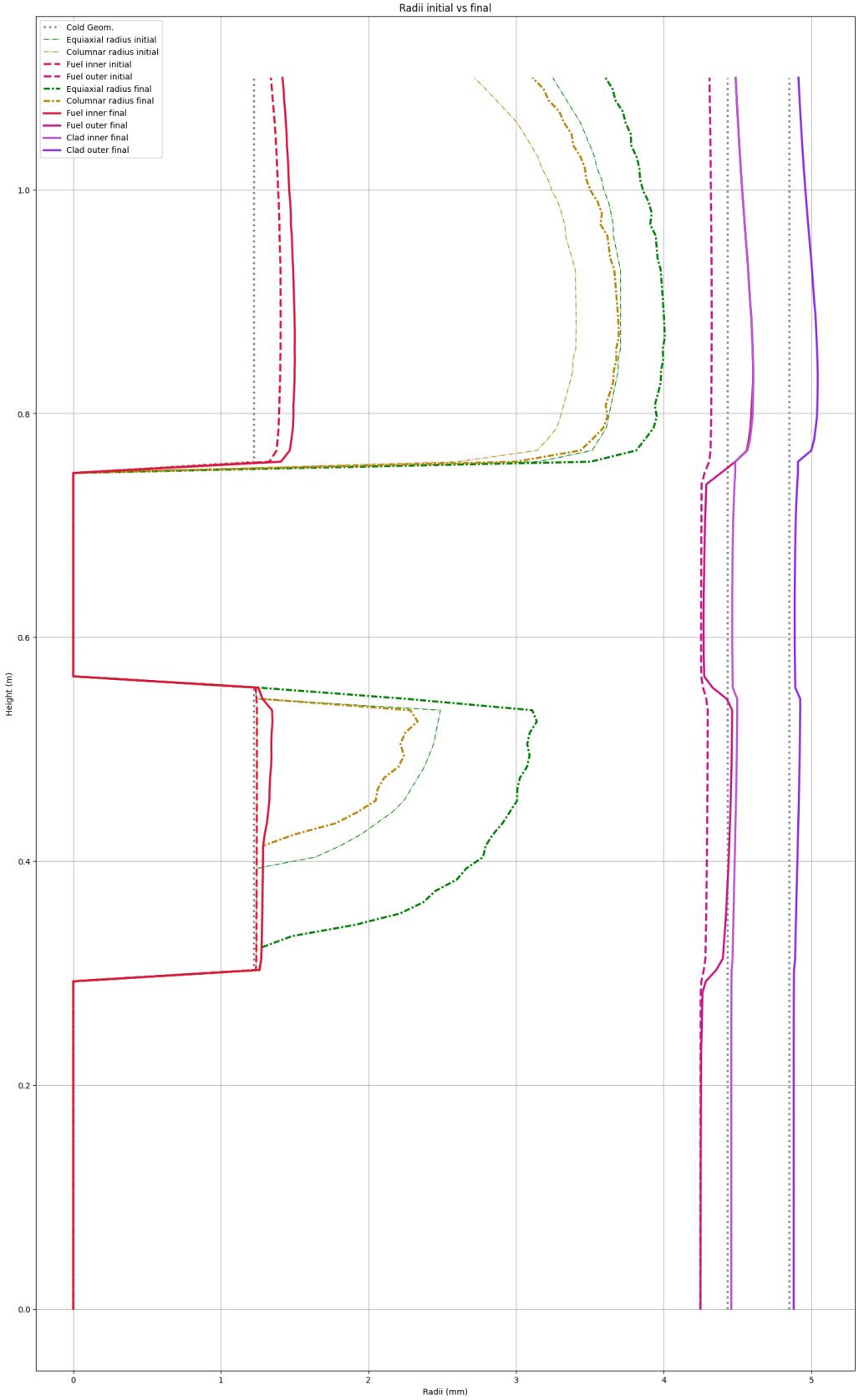

Figure 6: Axial Plot of the Radii

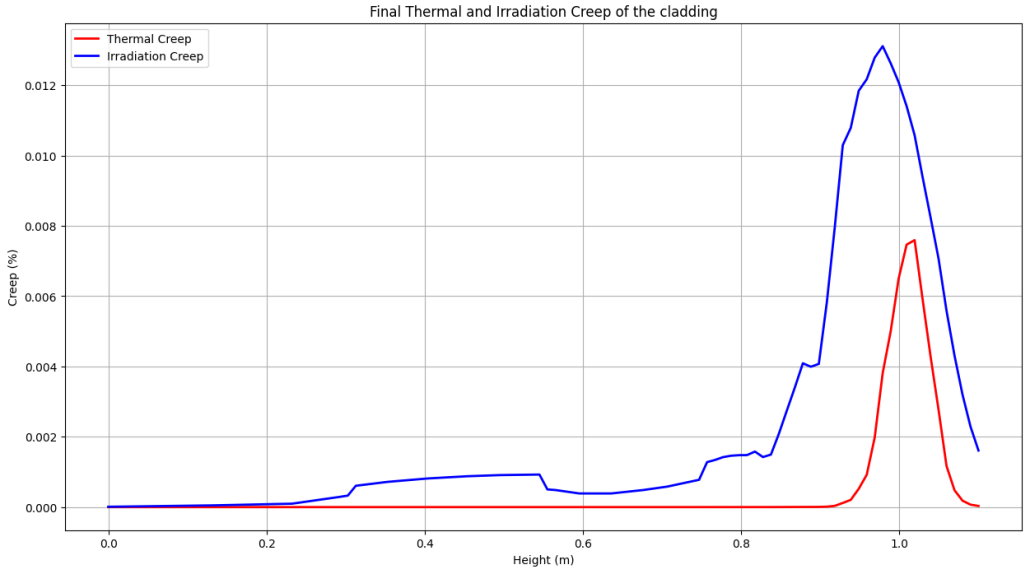

Figure 7: Irradiation and Thermal creep at the last day

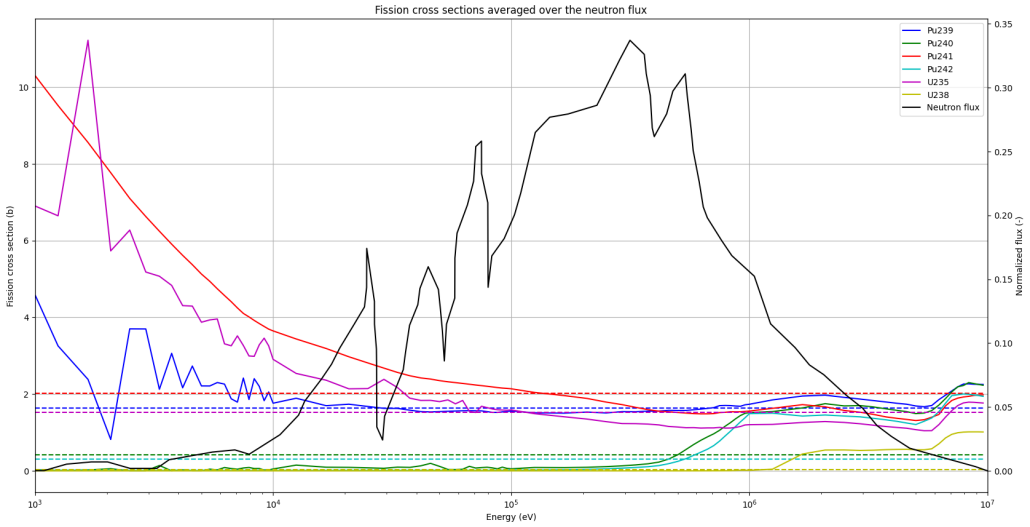

Figure 8: Fissile elements fission cross sections for group collapsing calculations

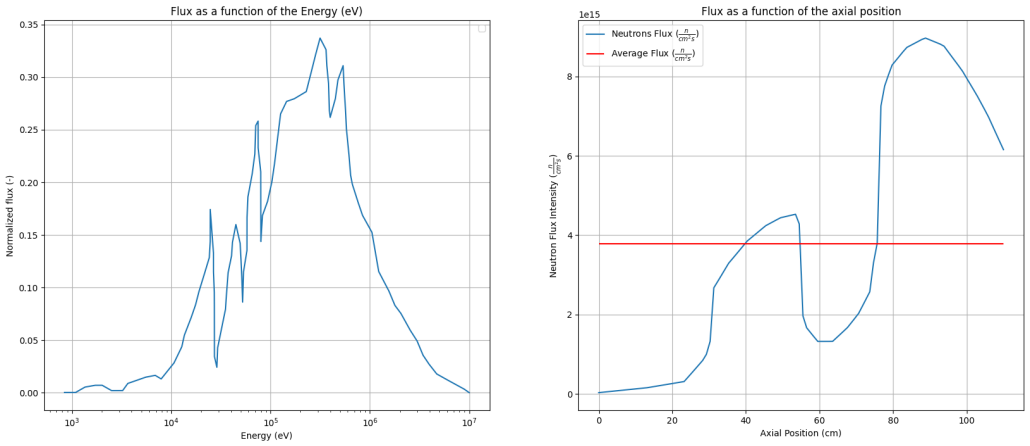

Figure 9: Neutron flux